ECCOMAS Congress 2016
VII European Congress on Computational Methods in Applied Sciences and Engineering
M. Papadrakakis, V. Papadopoulos, G. Stefanou, V. Plevris (eds.)
Crete Island, Greece, 5–10 June 2016

TOPOLOGY OPTIMIZATION FOR ADDITIVE MANUFACTURING WITH CONTROLLABLE SUPPORT STRUCTURE COSTS

Matthijs Langelaar

Delft University of Technology
Mekelweg 2, 2628 CD Delft, the Netherlands
e-mail: m.langelaar@tudelft.nl

Keywords: Topology optimization, additive manufacturing, overhang angle, support structures, self-supporting designs, manufacturing restrictions

Abstract. *Advances in additive manufacturing (AM) allow economical production of components with unprecedented geometric complexity. This offers exciting opportunities for innovative designs, and particularly topology optimization has been identified as a key technique to fully exploit the capabilities of AM. However, also AM involves manufacturing restrictions, such as limitations on the inclination of overhanging parts. To deal with this problem, either sacrificial supporting structures can be added during the process, or only self-supporting designs can be considered. Both approaches have disadvantages, as support structures add material and post-processing costs, while demanding exclusively self-supporting designs may impose strong restrictions on achievable performance. With current methods, designers are limited to a choice between these two extremes. To open up a wider range of designs, this paper presents and demonstrates a topology optimization formulation that allows the designer to find trade-off solutions between design performance and support structure costs, considering both printing and removal costs.*

1 INTRODUCTION

Additive manufacturing (AM) processes such as Selective Laser Melting (SLM) or Electron Beam Melting (EBM) allow economic fabrication of metal components with unprecedented geometric complexity [1]. This offers exciting opportunities for innovative designs, and particularly topology optimization (TO) has been identified as a key technique to fully exploit the capabilities of AM [2, 3, 4]. However, there are still geometric restrictions that must be taken into account. An important restriction that applies to popular powder-bed processes such as SLM and EBM, is that the inclination of printable overhanging parts with respect to the build plate is limited. This limitation is associated with a critical overhang angle, that typically amounts to 45° [5, 6].

Current practice is to first generate an optimized design using TO, and to subsequently find a part orientation that meets the overhang restriction. However, complex parts often lack a fully printable orientation. In that case, either the part must be modified, or sacrificial support structures must be printed together with the part itself (see Fig. 1(a)), and removed afterwards. The first option reduces part optimality, while the latter adds material and machining costs. A more preferable approach would be to include the AM restrictions in the TO process, making the subsequent steps unnecessary.

As a remedy, authors have explored the idea to e.g. optimize the addition of supporting structures, that become permanent parts of the final component [7]. Unfortunately this affects its optimality. Others have taken steps to identify overhang angles already during optimization, in order to generate fully self-supporting optimized designs [8, 9]. Still it was found that the previously published methods leave room for the optimization process to produce inadmissable structures.

To address this problem, this contribution first summarizes our approach to include the critical overhang angle restriction in the TO process. This approach utilizes a simplified AM fabrication model, that is applied in every TO iteration to transform a blueprint design layout into an as-printed part [10, 11]. The AM model is defined in a continuous, differentiable way, and sensitivities of the modeled AM operation can be computed efficiently. Applying TO including this AM fabrication model results in optimized designs that are fully printable, and rigorously comply with the overhang angle limitation. The necessary design modifications however may result in performance reduction compared to freely optimized parts, as illustrated by Fig. 1(b).

In the outlined approach, designers do not have an option to exercise control over the trade-off between performance reduction and support structure costs, which is restrictive. Building on the mentioned AM fabrication model, we therefore propose a TO problem formulation that allows for the simultaneous design of the actual part and the support structures required for its

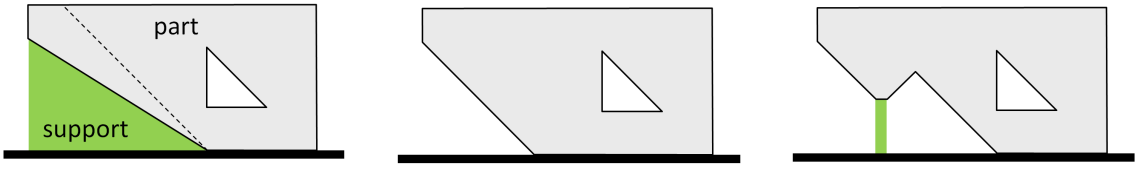

a) Unrestrained design b) Self-supporting design c) Trade-off design

Figure 1: Schematic 'Design for AM' options: a) parts optimized without considering AM restrictions typically require additional support material, b) fully self-supporting designs may show reduced performance / higher mass, c) the method proposed in this paper finds a compromise solution that balances part performance and support costs.

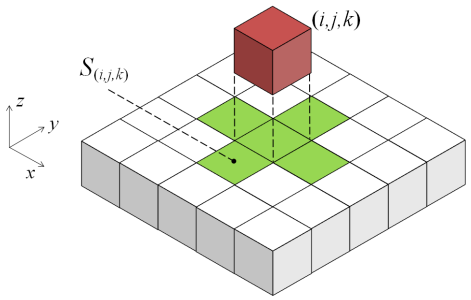

Figure 2: Definition of 3D AM filter, assuming the z-direction as the build direction. The green region $S_{(i,j,k)}$ denotes the supporting region of a red element at position (i, j, k) in a mesh. When insufficient printed material is present in this region, element (i, j, k) cannot be printed.

fabrication. The designer can specify costs associated to the printing of added support material, as well as costs for the machining effort required to remove a given amount of supports. Depending on these costs, the optimization finds the best trade-off between reduction in performance due to part adaptation, and added costs related to support structures (Fig. 1(c)). This allows for a controllable, rational approach to TO for AM, that enables the designer to find optimal designs in terms of cost and performance.

In the following, Section 2 introduces the AM fabrication model and the proposed trade-off formulation, followed by several 3D numerical examples in Section 3 and concluding remarks in Section 4.

2 FORMULATION

2.1 Printable volume detection

In order to detect which parts of a design require additional support, an operation is needed to identify the printable part of a given design layout. This is achieved by applying a simplified AM process simulation, that determines which parts of a layer are printable given the printable parts of the underlying layer. We distinguish two interrelated density values per element: a *blueprint density* b, expressing the material layout specified by the optimizer, and a *printed density* p, indicating the actually printable structure. The following subsections summarize the definition of this AM filter and its sensitivity analysis, for a more in-depth discussion the reader is referred to [10, 11].

2.1.1 AM filter definition

The simplified AM process model is defined on a structured grid, as depicted in Fig. 2. An element at position (i, j, k) is associated with a support region $S_{(i,j,k)}$, consisting of the element directly underneath and its four neighbours. The maximum printed density in $S_{(i,j,k)}$ determines the maximum printable density it can support. Mathematically this is expressed by:

$$p_{(i,j,k)} = \min\left(b_{(i,j,k)}, \max(p \in S_{(i,j,k)})\right). \tag{1}$$

By definition, the base layer ($k = 1$) is fully supported by the baseplate and thus fully printable: $p_{(*,*,1)} \equiv b_{(*,*,1)}$. In all subsequent layers, Eq. 1 is applied by sweeping through the domain in the build direction. In order to make this operation continuously differentiable, the min and max operators are replaced by smooth approximations $\breve{s}$ and $\hat{s}$. Further details are given in [10].

2.1.2 Sensitivity analysis under AM filter

A response f is evaluated on the printed part $\mathbf{p}$, which is indirectly defined by $\mathbf{b}$, i.e. $f = f(\mathbf{p}(\mathbf{b}))$. Sensitivities $\partial f/\partial \mathbf{p}$ are readily obtained, e.g. using adjoint sensitivity analysis. For gradient-based optimization, sensitivities in terms of $\mathbf{b}$ are required, which can be computed by:

$$\frac{\partial f}{\partial \mathbf{b}} = \frac{\partial f}{\partial \mathbf{p}}\frac{\partial \mathbf{p}}{\partial \mathbf{b}} = \frac{\partial f}{\partial \mathbf{p}}\mathbf{J}_{pb} \tag{2}$$

The Jacobian $\mathbf{J}_{pb}$ is not sparse and unattractive to compute in full, from a numerical point of view. Instead, we opt for an adjoint formulation. Using the AM filter definition $\mathbf{p}_k = \breve{s}(\mathbf{b}_k, \hat{s}(\mathbf{p}_{k-1}))$, where k is a layer index, it is found that, for layers $k > 1$:

$$\frac{\partial f}{\partial \mathbf{b}_k} = \boldsymbol{\lambda}_k^T \frac{\partial \breve{s}}{\partial \mathbf{b}_k}, \tag{3}$$

$$\boldsymbol{\lambda}_k^T = \frac{\partial f}{\partial \mathbf{p}_k} + \boldsymbol{\lambda}_{k+1}^T \frac{\partial \breve{s}}{\partial \mathbf{p}_k} \qquad \text{for } 1 < k < n, \tag{4}$$

$$\boldsymbol{\lambda}_n^T = \frac{\partial f}{\partial \mathbf{p}_n}, \tag{5}$$

with n indicating the number of layers. For the base layer, simply $\partial f/\partial \mathbf{b}_1 = \partial f/\partial \mathbf{p}_1$. Eqs. 3-5 are inexpensive to evaluate, by sweeping layerwise through the domain from the top layer back to the base.

2.2 Cost/performance trade-off

2.2.1 Problem formulation

The described AM filter rigorously eliminates designs that require support structures for overhanging sections from the design space. However, imposing these restrictions generally results in lower performance. In many cases designers may instead seek a trade-off solution, where the added costs of support material and its removal are balanced against a smaller reduction in performance. This can be achieved using the AM filter introduced in Section 2.1.1, by considering the blueprint design as a combination of the actual part and additional support structures. To do so, we introduce two new design fields: $\mathbf{d}$ representing the density distribution of the actual design, and $\mathbf{s}$ indicating the distribution of support material in the domain. The blueprint design then consists of the union of $\mathbf{d}$ and $\mathbf{s}$, which can be approximated as:

$$b_{(i,j,k)} = \hat{s}\left(d_{(i,j,k)}, s_{(i,j,k)}\right). \tag{6}$$

Next, this blueprint field is processed by the AM filter, producing an as-printed geometry $\mathbf{p}(\mathbf{b})$. This however consists of regions that are only included as support material, and regions that belong to the actual component. The component field $\mathbf{c}$ can be extracted by taking the intersection with the actual design $\mathbf{d}$, i.e.:

$$c_{(i,j,k)} = \breve{s}\left(p_{(i,j,k)}(\mathbf{b}), d_{(i,j,k)}\right). \tag{7}$$

Performance is evaluated on the component geometry $\mathbf{c}$. Moreover, the amount of support material follows from $\mathbf{s}$, and we assume the support removal effort to be proportional to a measure of the part-support interface. The latter is given by the intersection between $\mathbf{d}$ and $\mathbf{s}$, i.e.:

$$i_{(i,j,k)} = \breve{s}\left(d_{(i,j,k)}, s_{(i,j,k)}\right). \tag{8}$$

A density filter is used, hence some overlap exists between $\mathbf{d}$ and $\mathbf{s}$, which allows this definition to be used. To summarize, the formulation now involves two fields controlled by the optimizer: the actual design $\mathbf{d}$ and the supports $\mathbf{s}$. In addition, we have defined a blueprint design for the printer $\mathbf{b}$, the printed geometry $\mathbf{p}$, the component $\mathbf{c}$ and the support/part interface $\mathbf{i}$. Note that other choices are possible, e.g. the actually printed support geometry could be defined similar to $\mathbf{c}$. The present formulation was chosen for its relative simplicity.

This leads to the following optimization problem:

$$\begin{aligned} \min_{\mathbf{d},\mathbf{s}} \quad & f(\mathbf{c}) + c_s V_s(\mathbf{s}) + c_r V_i(\mathbf{d},\mathbf{s}) \\ s.t. \quad & g_i(\mathbf{c}) \leq 0 \\ & 0 \leq \{\mathbf{d},\mathbf{s}\} \leq 1. \end{aligned} \tag{9}$$

Here f denotes the component performance indicator to be optimized, c_s and c_r are cost factors related to the amount of support material and removal costs, respectively, and g_i are certain constraints imposed on the component. V_s and V_i denote the volume of support material and support-component interface regions as defined by Eq. 8, relative to the design domain. By choosing the cost factors adequately in relation to the performance, different trade-off designs can be generated. For very high cost factors, the design tends towards a fully printable geometry without any support material. However, that result is easier to achieve by applying the AM filter to $\mathbf{d}$ only, and omitting the support variables. The benefit of this refined formulation is that trade-off solutions can be found, where some support material is used in those places, where further design adaptation would result in undesirable performance reductions. The influence of different choices of c_s and c_r is demonstrated using numerical examples in Section 3.

2.2.2 Sensitivity analysis

The responses involved in Eq. 9 in part depend on the component performance. The component geometry is obtained from the actual design combined with the printed part (Eq. 7), which itself results from the blueprint design, given by the actual design field and the support material: $g_i(\mathbf{c}(\mathbf{p}(\mathbf{b}(\mathbf{d},\mathbf{s}))),\mathbf{d})$. Given these dependencies, the design sensitivities of the responses involved in Eq. 9 follow from application of the chain rule as:

$$\begin{aligned} \frac{\partial f}{\partial \mathbf{d}} &= \frac{\partial f}{\partial \mathbf{c}}\left(\frac{\partial \mathbf{c}}{\partial \mathbf{p}}\frac{\partial \mathbf{p}}{\partial \mathbf{b}}\frac{\partial \mathbf{b}}{\partial \mathbf{d}} + \frac{\partial \mathbf{c}}{\partial \mathbf{d}}\right) + c_r \frac{\partial V_i}{\partial \mathbf{i}}\frac{\partial \mathbf{i}}{\partial \mathbf{d}}, \\ \frac{\partial f}{\partial \mathbf{s}} &= \frac{\partial f}{\partial \mathbf{c}}\frac{\partial \mathbf{c}}{\partial \mathbf{p}}\frac{\partial \mathbf{p}}{\partial \mathbf{b}}\frac{\partial \mathbf{b}}{\partial \mathbf{s}} + c_s \frac{\partial V_s}{\partial \mathbf{s}} + c_r \frac{\partial V_i}{\partial \mathbf{i}}\frac{\partial \mathbf{i}}{\partial \mathbf{s}}, \\ \frac{\partial g_i}{\partial \mathbf{d}} &= \frac{\partial g_i}{\partial \mathbf{c}}\left(\frac{\partial \mathbf{c}}{\partial \mathbf{p}}\frac{\partial \mathbf{p}}{\partial \mathbf{b}}\frac{\partial \mathbf{b}}{\partial \mathbf{d}} + \frac{\partial \mathbf{c}}{\partial \mathbf{d}}\right), \\ \frac{\partial g_i}{\partial \mathbf{s}} &= \frac{\partial g_i}{\partial \mathbf{c}}\frac{\partial \mathbf{c}}{\partial \mathbf{p}}\frac{\partial \mathbf{p}}{\partial \mathbf{b}}\frac{\partial \mathbf{b}}{\partial \mathbf{s}}. \end{aligned}$$

The individual derivatives follow from the expressions given in Section 2.2.1 and derivatives of the chosen smooth approximations $\breve{s}$ and $\hat{s}$. The term expressing the dependence of the printed part with respect to the blueprint design, $\partial\mathbf{p}/\partial\mathbf{b}$, is not computed in full: instead the more efficient adjoint sensitivity transformation given by Eqs. 3-5 is applied.

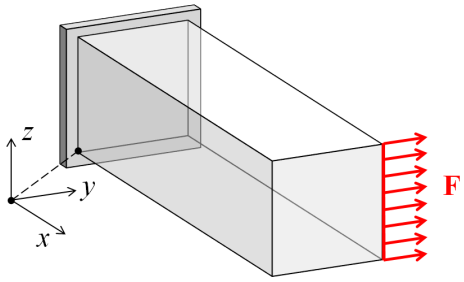

Figure 3: Cantilever beam test case used in numerical compliance minimization tests. The design domain is meshed with $150\times50\times50$ elements, and a load of 1000 N is distributed over the right front edge. The z-direction is chosen as build direction.

3 NUMERICAL EXAMPLES

3.1 Test case

In this paper, to demonstrate the additional freedom that the proposed trade-off formulation offers to the designer, we consider a cantilever beam optimized for minimum compliance, as depicted in Fig. 3. We assume that the orientation of the part has been specified a priori, and deliberately choose an orientation that is not favorable for the design, in order to clearly demonstrate the trade-off solutions the optimization process must find. Note that in real applications, part orientations are also often predetermined, due to demands on surface quality, post-processing operations, chamber size or costs (build height).

We solve the classical compliance minimization problem, under a 50% volume constraint, using the formulation given by Eq. 9. The problem is solved for different combinations of support- and removal costs c_s and c_r. Cube-shaped trilinear isoparametric finite elemens have been used, and the optimization has been performed using the Method of Moving Asymptotes [12]. Density filtering was used to define the $\mathbf{d}$ and $\mathbf{s}$ fields from the fundamental optimization variables, with a filter radius of 1.5 times the element edge length. 3D results are depicted by their isosurface, extracted at a density level 0.3.

3.2 Results

3.2.1 Reference designs

First we consider two extreme cases as reference designs: the unrestrained case, where no AM restrictions are applied (cost factors set to zero), and the fully self-supporting case (cost factors set to 10^3). This corresponds to the cases illustrated in Fig. 1(a) and (b). To interpret the cost factors, note that the numerical magnitude of the optimal compliance is around 25.

The obtained designs are depicted in Fig. 4. Note the presence of ample amounts of support material in Fig. 4(a), even coinciding with the actual component material. There is no driving force for the optimizer to be economical with support structures, hence they appear all throughout the domain. In contrast, the case with costly supports results in a fully self-supporting design, with no support structures at all (Fig. 4(b)). The compliance of the unrestrained case is $C_u = 25.55$, and that of the fully self-supporting case $C_{ss} = 27.63$. Requiring the entire part to meet the AM restrictions has worsened its compliance performance for this problem by 8%.

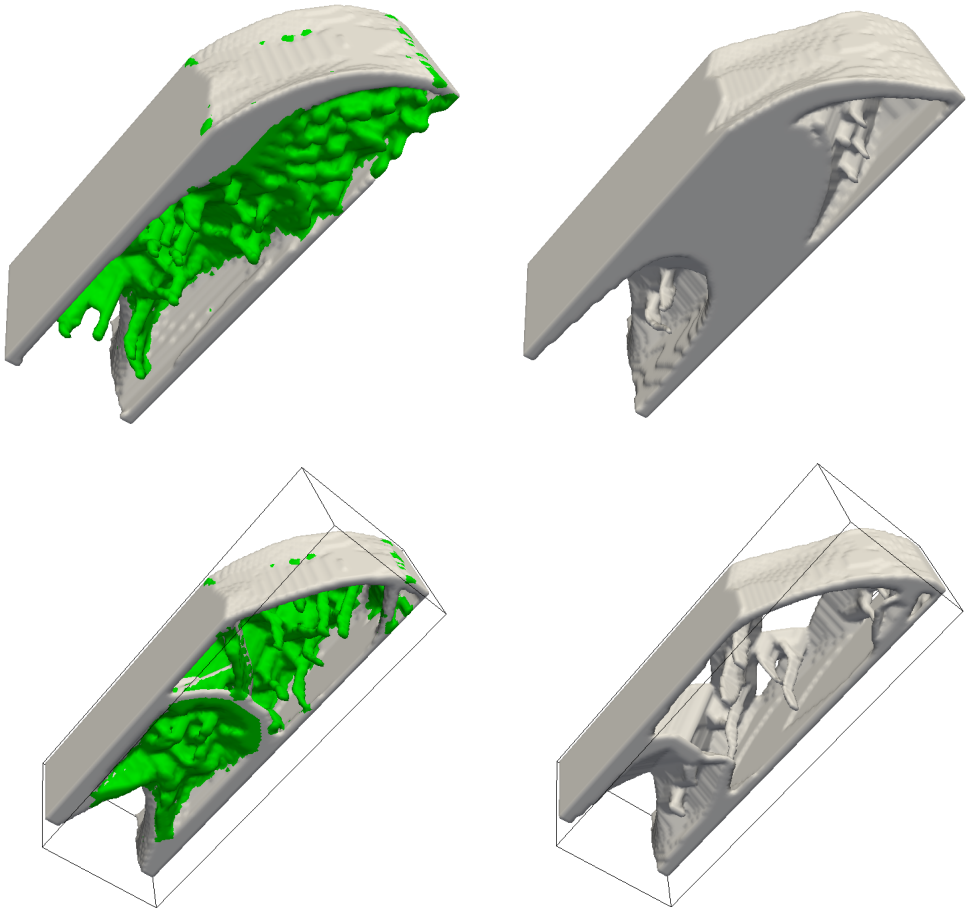

a) Unrestrained design b) Fully self-supporting design

Figure 4: Cantilever beam designs obtained in compliance minimization using either a) no AM restrictions or b) requiring the final design to meet the overhang restrictions everywhere, in full and cutaway view. Sacrificial support material is depicted in green, the actual component in white. The part is viewed from below the baseplate, in the printing direction.

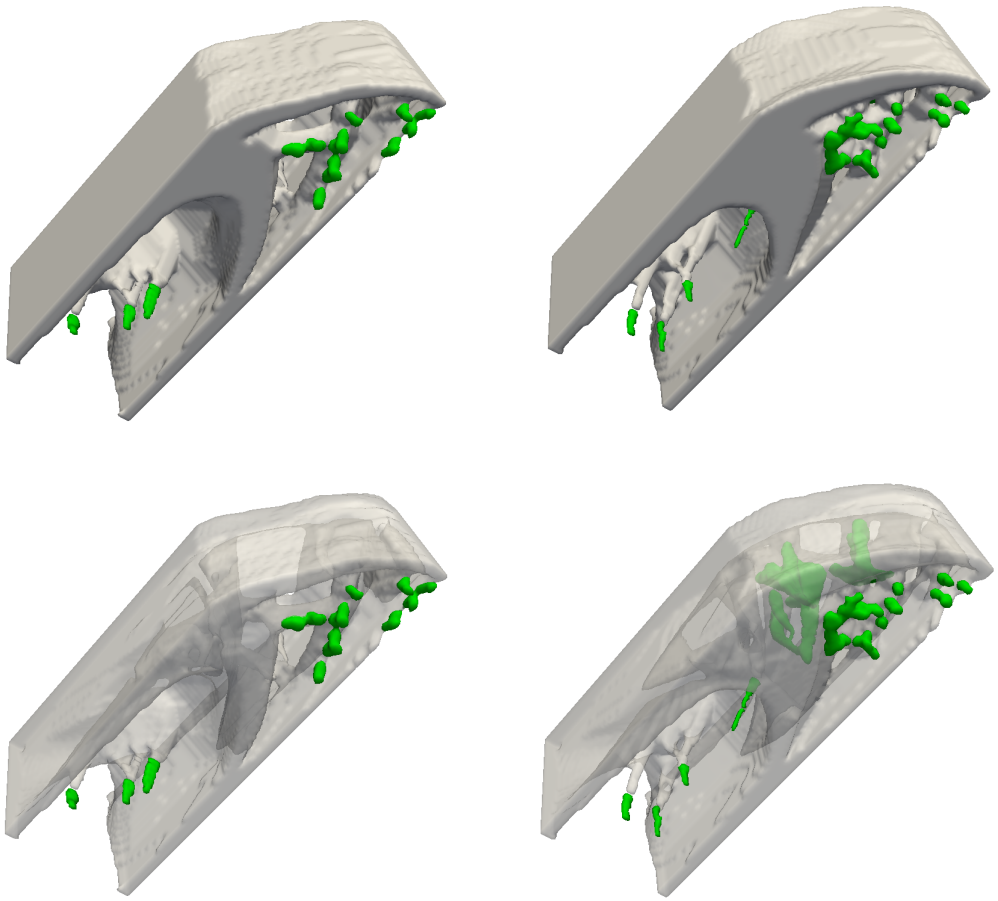

a) $c_s = 10, c_r = 0$ (no removal costs) b) $c_s = 0, c_r = 10$ (no support material costs)

Figure 5: Beam designs obtained considering either a) no removal costs, or b) no support material costs. Sacrificial support material is depicted in green, and the actual component in white, opaque and semi-transparent. The part is viewed from below the baseplate, in the printing direction.

3.2.2 Trade-off designs

Next we present various results that illustrate trends of the effect of the cost factors on the obtained designs. At the moment we have no access to realistic cost calculations, hence the focus of this study is purely on determining if the formulation has the intended characteristics. First, we consider the support and removal costs separately. Although they have different units, both are set numerically to 10.0 with their counterpart equal to zero. Resulting designs are depicted in Fig. 5.

The amount of support material employed by the optimizer is less than that when no costs were associated to its usage (Fig. 4(a)); instead, it is applied more sparingly to specific locations where the costs of either support material or interfaces balances with the gain or loss in performance. Especially in the plots with transparent component geometry in Fig. 5 it is seen that also a difference exists between restricting material usage or interface area: Fig. 5(b) clearly contains more support material. In terms of compliance, the $c_r = 0$ case is close to the fully self-supporting case C_{ss}, while the $c_s = 0$ case does slightly better: 7% higher than C_u, which corresponds to the higher support material usage seen for this design. Note that the chosen cases are not directly comparable: the cost factor 10.0 has a different meaning when

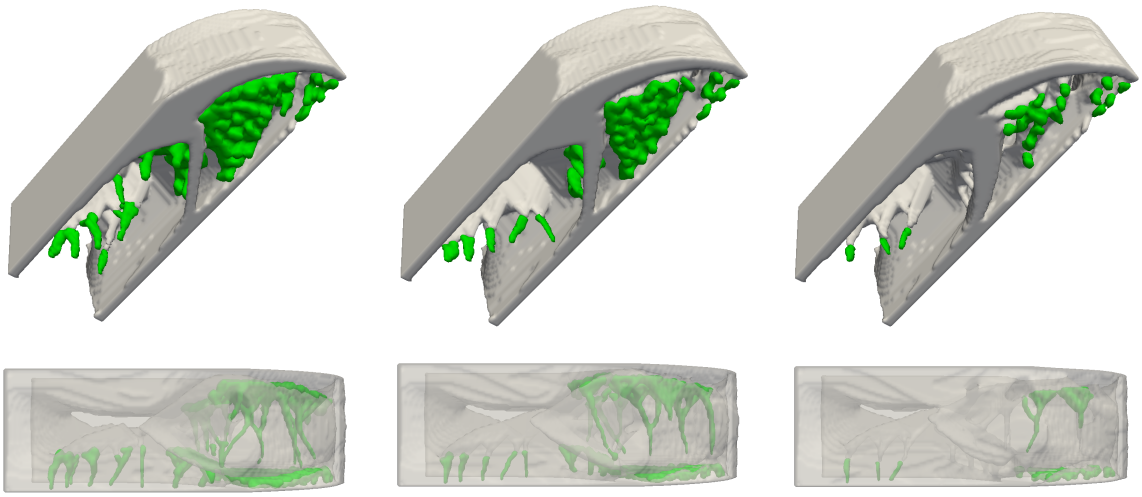

a) $c_s = 0.1, c_r = 1$ b) $c_s = 0.5, c_r = 5$ c) $c_s = 2.5, c_r = 25$

Figure 6: Beam designs obtained considering various levels of support and removal costs. Sacrificial support material is depicted in green, and the actual component in white, opaque and semi-transparent. The part is viewed from below the baseplate, in the printing direction (top row) and from above towards the baseplate (bottom row).

applied to volume or area. Nevertheless, the observed trends confirm that this formulation is able to distinguish different cost aspects.

Next, the ratio between support material and removal costs is fixed to 1:10, and different cost levels are considered. Results are depicted in Fig. 6. It is seen that changing the cost factors leads to adjustments in the optimized design, with the employed amount of support material decreasing with increasing costs.

Relative compliances of these three cases are 1.6%, 3.5% and 4.6% worse than the unrestrained design (C_u, Fig. 4(a)), but all clearly better than forcing the design to be fully self-supporting, which yielded an 8% performance drop (C_{ss}, Fig. 4(b)). This is as expected: adding more severe restrictions leads to further reductions in achievable performance. Note also that the support material layout as seen in the transparent plots shown in Fig. 6 is optimized in the process as well: to limit the amount of sacrificial material, branches are formed that merge together to form a connection to the baseplate. In the present model, no stiffness requirements are taken into account for the support structures, but the problem formulation can in principle be extended with constraints related to the printed geometry field $\mathbf{p}$ as well.

4 DISCUSSION AND CONCLUSIONS

A new formulation that enables designers to find trade-off solutions when using topology optimization for additive manufacturing has been presented. It builds on a filter-based procedure to create exclusively self-supporting designs. While effective, for practical applications, a less restrictive approach that can find a rational compromise between part performance and production costs is often desired.

The presented formulation, employing a simple cost model considering support structure volume and removal costs, generates fully printable combinations of component and support geometry. As expected, optimized part performance decreased as support and removal costs increased. When applying realistic cost factors, this allows designers to properly balance performance and costs. The cost model itself is simple and should be seen as a placeholder for more

refined cost models for specific processes. Also, an important limitation is that the present procedure does not account for the accessibility of the interfaces that require machining for support removal. Even enclosed voids may occur in the designs. Therefore, engineering judgement is still necessary to evaluate the proposed solutions.

The examples confirm that enforcing full compliance with the AM process' overhang limitations comes at a cost in terms of part performance. In this case, the maximum difference amounted only to 8%, and in fact other part orientations do not result in performance reductions [11]. The examples are however only intended to illustrate the principle, that in general restrictions often reduce performance, and that the presented cost-based formulation offers a way to find a compromise.

The current method assumes a fixed part orientation, while in reality freedom may exist to reorient the part. This can be included in the present formulation by considering multiple optimizations with different orientations. However, this directly increases the computational effort, hence also here engineering insight in the selection of suitable orientations is required. Substantial gains or losses can result from part orientation choices, and including this aspect in the optimization is considered an important topic for future work.

REFERENCES

[1] E. Atzeni, A. Salmi, Economics of additive manufacturing for end-usable metal parts, The International Journal of Advanced Manufacturing Technology 62 (9-12) (2012) 1147–1155.

[2] C. Emmelmann, J. Kranz, D. Herzog, E. Wycisk, Laser additive manufacturing of metals, in: Laser Technology in Biomimetics, Springer, 2013, pp. 143–162.

[3] D. Rosen, Design for additive manufacturing: Past, present, and future directions, Journal of Mechanical Design 136 (9) (2014) 090301.

[4] T. Zegard, G. H. Paulino, Bridging topology optimization and additive manufacturing, Structural and Multidisciplinary Optimization 53 (2016) 175–192.

[5] R. Mertens, S. Clijsters, K. Kempen, J.-P. Kruth, Optimization of scan strategies in selective laser melting of aluminum parts with downfacing areas, Journal of Manufacturing Science and Engineering 136 (6) (2014) 061012.

[6] J. Kranz, D. Herzog, C. Emmelmann, Design guidelines for laser additive manufacturing of lightweight structures in TiAl6V4, Journal of Laser Applications 27 (S1) (2015) S14001.

[7] M. Leary, L. Merli, F. Torti, M. Mazur, M. Brandt, Optimal topology for additive manufacture: A method for enabling additive manufacture of support-free optimal structures, Materials & Design 63 (2014) 678–690.

[8] D. Brackett, I. Ashcroft, R. Hague, Topology optimization for additive manufacturing, in: Proceedings of the Solid Freeform Fabrication Symposium, Austin, TX, 2011, pp. 348–362.

[9] A. Gaynor, J. Guest, Topology optimization for additive manufacturing: considering maximum overhang constraint, in: 15th AIAA/ISSMO multidisciplinary analysis and optimization conference, 2014, pp. 16–20.

[10] M. Langelaar, An additive manufacturing filter for topology optimization of print-ready designs, Structural and Multidisciplinary Optimization, in review (2016, forthcoming).

[11] M. Langelaar, Topology optimization of 3D self-supporting structures for additive manufacturing, Additive Manufacturing, in review (2016, forthcoming).

[12] K. Svanberg, The method of moving asymptotes - a new method for structural optimization, International Journal for Numerical Methods in Engineering 24 (2) (1987) 359–373.